

A correlation-based central difference image correction (CDIC) method and application in a four-roll mill flow PIV measurement

S.T. Wereley, L. Gui

42

Abstract An experiment is conducted in a four-roll mill to verify a novel particle image velocimetry (PIV) recording evaluation method that combines the advantages of central difference interrogation and an image correction technique. Simulations and experiments in the four-roll mill geometry demonstrate that the central difference image correction method described in this paper can not only avoid the bias error resulting from the curvature and high-velocity-gradient flow but also effectively reduce the random error resulting from particle image distortion. Two image correction schemes and two base algorithms are discussed. A four-point image correction scheme is suggested on the basis of the traditional correlation-based interrogation algorithm to enable a fast, high-accuracy evaluation of PIV recordings in complex flows. In addition, the PIV experiment accurately determines the velocity field in the four-roll mill and confirms the linear distributions of the velocity components and the roller speed.

1 Introduction

The four-roll mill is a device proposed by Taylor (1934) to study the breakup of small droplets in a viscous straining velocity field. It can produce a purely two-dimensional extensional flow and has proven to be a popular instrument for studying drop deformation (Rumscheidt and Masno 1961; Higdon 1993), birefringence in polymer solutions (Guller and Leal 1981), and flow-induced crystallization in polymer melts (Torza 1975). Bentley and Leal

(1986a, 1986b) designed a computer-controlled four-roll mill capable of producing arbitrary linear flow fields, holding droplets stationary in the center of the flow cell, and causing two droplets to interact. In the present work, the particle image velocimetry (PIV) technique is used to investigate the flow in a computer-controlled four-roll mill. The four-roll mill generates a typical curvature flow, which causes significant image pattern distortion in the PIV recordings. In order to investigate the flow structure near the center of the device, i.e., the very-low-velocity region, large time intervals are usually used, so that relatively large particle image displacements are produced in the PIV recording pairs outside of the flow center. Therefore, window shifting and image pattern correction are necessary for evaluating PIV recordings obtained in the four-roll mill PIV experiment.

Currently, adaptive discrete window shifting is widely used with the FFT-based correlation algorithm for reducing the evaluation error and with the image-pattern-tracking algorithms for increasing the spatial resolution. The adaptive window offset method, as typically implemented, can be referred to as the forward difference interrogation (FDI), because the second interrogation window is shifted in the forward direction of the flow by an amount equal to the mean displacement of the particle images initially in the first window. Details of the FDI technique are described by Keane and Adrian (1993), Willert (1996), Cowen and Monismith (1997), Westerweel et al. (1997), and Scarano and Riethmuller (1999). Although the FDI method leads to significant improvements in the evaluation quality of PIV recordings in many cases, there are still some potentially detrimental bias errors that cannot be avoided with FDI, for instance, the position deviation in flows with large velocity gradients and direction deviation in curvature flows. A central difference interrogation (CDI) method was initially introduced by Wereley et al. (1998) and further developed and explored by Wereley and Meinhart (2000, 2001), to avoid the shortcomings of FDI and increase the accuracy of the PIV measurement. When using CDI, the first and the second interrogation windows are shifted backward and forward, respectively, each by half of the expected particle image displacement. As multi-pass adaptive spatial-shifting techniques, both FDI and CDI require some iteration to achieve optimum results. When properly programmed, using CDI does not cost more computation time than FDI. Recent studies (Scarano and Rethmuller 2000; Sjö Dahl 1994; Sholl and Savas 1997; Lecordier et al. 2001; Gui and Wereley 2002) indicate that the bias and random errors of

Received: 28 December 2001 / Accepted: 15 July 2002

Published online: 1 November 2002

© Springer-Verlag 2002

S.T. Wereley, L. Gui (✉)
Mechanical Engineering, Purdue University,
West Lafayette, IN 47907-1288, USA
E-mail: lcgui@yahoo.com

Present address: L. Gui
Nationale Center for Physical Acoustics (NCPA),
University of Mississippi, Coliseum Drive,
P.O. Box 1848, University, MS 38677, USA

This work was supported by the Indiana 21st Century Research and Technology Fund and the Integrated Detection of Hazardous Materials (IDHM) Program – a Department of Defense project managed jointly by Center for Sensing Science and Technology, Purdue University, and Naval Surface Warfare Center, Crane, Indiana. Thanks to Derek Tretheway and Professor Gary Leal for making images from the four-roll mill experiments available to us.

the digital PIV recording evaluation can be reduced further by continuously shifting the interrogation window according to previous evaluations, and consequently, the peak-locking effect is minimized.

To account for the distortion of PIV image patterns in complex flow measurements, image correction techniques have been developed. The idea of image correction was first presented by Huang et al. (1993), and similar ideas were applied by Tokumaru and Dimotakis (1995), Fincham and Spedding (1997), Lin and Perlin (1998), Nogueira et al (1999, 2001), and Scarano (2002). In order to accelerate the evaluation, the authors combine a modified image correction method with the FFT-based correlation algorithm, so that the evaluation error resulting from the image pattern distortion can be effectively reduced with only little additional computation time, i.e., a fraction of the regular evaluation time. Named the central difference image correction (CDIC) method in this paper, the new evaluation algorithm combines ideas of CDI,

adaptive continuous window shifting and image correction, and enables a most reliable and accurate evaluation of digital PIV recordings. Details are provided below.

2 Description of the method

2.1 CDIC

The idea of CDIC is demonstrated in Fig. 1 by evaluating a synthetic PIV image pair near a strong vortex center with a 64×64 -pixel interrogation window and a 50% overlap. The velocity distribution on the 3×3 interrogation grid (Fig. 1a) consists of a translation movement (Fig. 1b) and distortion (Fig. 1c) instantaneously. When using the traditional cross-correlation algorithm, the evaluation sample pair is obtained with an interrogation window centered at the evaluation point, e.g., Fig. 1d and e for the central point of the 3×3 grid. The traditional correlation

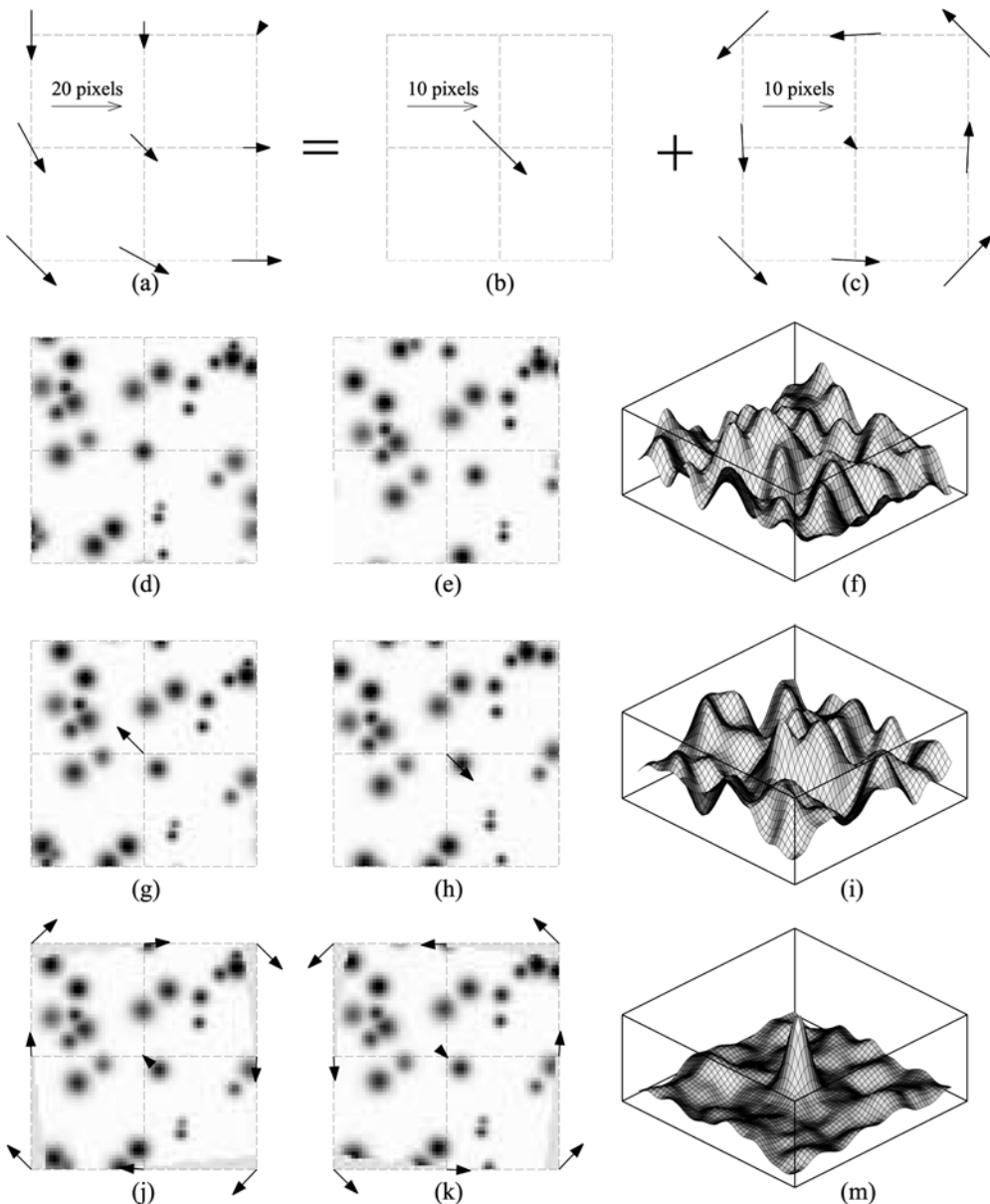


Fig. 1a–m. Interrogation window shift and image pattern correction

method works well in cases of small particle image displacement and relatively simple flow. However, in the current case, the image patterns in the sample pair do not match well, so that the correlation function (Fig. 1f) does not show a dominant peak for the particle image displacement. Considering the translation movement of the particle images in the evaluation sample pair, the interrogation windows for the first and second recording can be shifted backwards and forwards, respectively, to realize a CDI (see Fig. 1g and h), so that the image patterns match better to each other. However, the correlation function still does not present a very clear peak to reliably and accurately determine the particle image displacement (Fig. 1i). When considering the particle image distortion, i.e., pre-defining the image patterns forward and backwards respectively for the first and second evaluation sample (Fig. 1j and k) based on the known displacements at the nine grid points, a very good match of the image patterns is realized, so that a correlation function with a clear main peak is obtained (Fig. 1m). Although in this demonstration the window shifting and the image pattern correction are carried out in two steps, they can be realized in only one step in practical applications.

2.2

Interpolation of particle images

When using the FFT algorithm to accelerate the calculation, the correlation-based interrogation function is usually written as

$$\Phi(m, n) = \sum_{i=1}^M \sum_{j=1}^N g_1(i, j) \cdot g_2(i + m, j + n), \quad (1)$$

where g_1 and g_2 are gray value distributions of the two evaluation samples, which are restricted in a rectangular interrogation window of size of $M \times N$ pixels. For traditional correlation algorithms with or without discrete window shifting, $g_1(i, j)$ and $g_2(i, j)$ are extracted directly from the discrete gray value distributions of the PIV recording pair $G_1(i, j)$ and $G_2(i, j)$, respectively. However, when using CDIC, the shifts of pixels in the interrogation window are not limited to discrete integer values and, in most cases, are not a constant. We assume that the displacement of the image pattern at pixel (i, j) in the interrogation window is determined as $X(i, j)$ and $Y(i, j)$. The following bilinear interpolation function is used for determining the correlated function:

$$g(i, j) = (1 - x) \cdot (1 - y) \cdot G(i + I, j + J) + x \cdot (1 - y) \cdot G(i + I + 1, j + J) + y \cdot (1 - x) \cdot G(i + I, j + J + 1) + x \cdot y \cdot G(i + I + 1, j + J + 1), \quad (2)$$

wherein (I, J) and (x, y) are integer pixels and non-negative sub-pixel values, respectively; for $g=g_1$ and $G=G_1$: $I+x=-0.5X$, $J+y=-0.5Y$; for $g=g_2$ and $G=G_2$: $I+x=0.5X$, $J+y=0.5Y$. If $G(i, j)$ is limited in the $M \times N$ -pixel sampling window, there may not be enough information to completely fill the rectangular interrogation window, e.g., in Fig. 1j and k there are vacancy areas near the edges of the interrogation windows. However, since $G(i, j)$ is defined in

the whole image plane, the interrogation window can completely be filled with PIV recording information in most cases. When the evaluation point is chosen at the edges of the PIV recording, padding or mask techniques (Gui and Merzkirch 1996, 1998) can be used to deal with the vacancy area problem.

The bilinear interpolation is used here for the CDIC scheme, because it is simple, stable and of high speed. A test is conducted to quantify the added evaluation error caused by the interpolation. In this test, synthetic PIV recording pairs of different diameters are generated with a uniform particle image displacement of 0.5 pixels. The brightness of the particle image, i.e., the gray value in its center, is 250; the particle image number density is $0.0195 \text{ pixel}^{-1}$. An interrogation window of 32×32 pixels is used to evaluate these synthetic PIV recording pairs using the correlation-based interrogation algorithm without and with a window shift, respectively, of exactly 0.5 pixels. In the latter case, the particle image displacement to be determined is zero and the bilinear interpolation is used to reconstruct the particle images in the shifted second interrogation window. Since the evaluation error of the correlation-based interrogation algorithm is zero at zero displacement for particle images without noises, the evaluation error in the case with 0.5-pixel window shift is considered to be the error resulting from the bilinear interpolation. The evaluation errors added by the interpolation at different particle image diameters (δ_{intp}) are given in Fig. 2, which is normalized with the evaluation error of the correlation-based interrogation algorithm without window shift (δ_{corr}). In this test, the interpolation error is less than 10% of the correlation error when the particle image diameter is more than 2 pixels.

2.3

Image correction schemes

Because the particle image displacement (X, Y) is unknown before evaluation, initial values are taken to be zero or determined with previous knowledge of the flow. Then the evaluation is iterated until the convergence condition is fulfilled. Instead of determining the particle image displacement (X, Y) at every pixel in the interrogation window like the conventional image correction methods, displacements at the four corners (four-point method) or

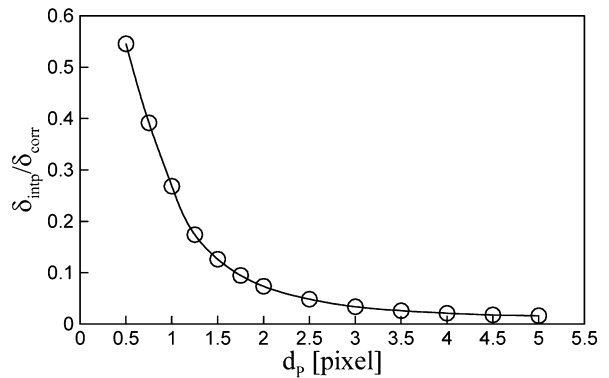


Fig. 2. Evaluation error caused the bilinear image interpolation (δ_{intp}) normalized with the correlation interrogation error without window shift (δ_{corr})

also at five center points (nine-point method) of the interrogation window are used to determine the correction of the distorted image patterns. For the four-point method, the interrogation window is taken as one rectangular cell, whereas for the nine-point method, there are four cells in the interrogation window. Within each rectangular cell, the displacement (X, Y) is determined with a bilinear interpolation function similar to Eq. 2. This simplification enables not only a fast image-corrected evaluation of the PIV recordings but also good convergence of the multi-pass evaluation algorithm. When using the four-point image correction method, an adjustment is made, so that the displacement in the window center determines the translation movement and the displacements at the four corners determine the particle image pattern distortion.

The convergence of the CDIC method is tested here using a synthetically generated PIV recording pair with given particle image displacement $X=5 \cos(j/256)$, $Y=5 \cos(i/256)$ pixels. The synthetic particle images have a Gaussian gray-value profile and are randomly distributed in the PIV recordings of size of $1,024 \times 1,024$ pixels. The brightness of the particle image is $130 \sim 250$; the particle image diameter is $2 \sim 5$ pixels; the particle image number is 20,480, i.e., approximately 20 particles in the 32×32 -pixel interrogation window. This PIV recording pair is evaluated by using the above-described four- and nine-point image correction method, respectively, and the convergence errors and evaluation errors are given in Fig. 3 in dependence on the iteration number. Here the convergence error is defined as the RMS difference between the particle image displacements obtained in current and last iteration, and a tolerance is given as stopping criterion of the iteration cycle. The RMS evaluation error can be determined because the real displacements of particle images are known in the simulated recording pair. The evaluation is conducted with a uniform grid and produces about

4,000 displacement vectors. As shown in Fig. 3a, the evaluation procedure of the four-point and nine-point method converges after four and five iterations, respectively, with a tolerance of 0.02 pixels. Figure 3b shows that the evaluation with the four-point method converges at a much lower RMS error than that of the nine-point method. In an ideal case, evaluations are also conducted with given particle image displacements for the image correction without iterations, and the results show that the evaluation error of the nine-point method is somewhat smaller than that of the four-point. However, the high accuracy of the nine-point method in the ideal case cannot be achieved in practical applications, where the particle image displacements are usually unknown. This may be explained with that the additional degrees of freedom in the nine-point fit allow the particle image patterns to be matched well in the presence of small displacement deviations.

As indicated in Fig. 3, four or five iterations are usually necessary for CDIC to complete the evaluation. In comparison to the FFT-based discrete window-shifting techniques, the new algorithm needs 75% more computation time because of the interpolations. For complex flows, some validation, interpolation, and smooth tools may be necessary between iterations. Sometimes, a proper estimation of initial displacements for the first iteration is necessary. In order to avoid too much computation time, a number limit can be set to jump out of the iteration cycle before the convergence condition is fulfilled.

2.4

Base algorithms of the CDIC method

In the above discussions, the CDIC method is constructed on the basis of the traditional correlation-based interrogation algorithm, i.e., the two evaluation samples (windows) have the same size. Recently, another correlation scheme, called correlation-based tracking here, has been commonly used. The correlation-based tracking correlates a smaller window with a larger window. Theoretically, the evaluation error of the correlation-based interrogation algorithm is zero at zero displacement (Westerweel et al. 1997) and usually much smaller than that of the correlation-tracking algorithm when the particle image displacement is within ± 0.2 pixel (Gui and Merzkirch 2000; Gui and Wereley 2002). However, it has much larger evaluation errors than the correlation-based tracking algorithm at large particle image displacements. Even though the correlation-based interrogation algorithm is improved by applying a discrete window-shifting technique, it is usually considered a faster but less accurate algorithm than the correlation-based tracking. The CDIC method applies a multi-pass scheme that makes the magnitude of the particle image displacement very small ($\ll 0.2$ pixel) after a few iterations, so that a higher accuracy can be achieved with the correlation-based interrogation algorithm than with the correlation-based tracking algorithm.

To compare the performances of the two correlation schemes in combination with CDIC, the first test is conducted with a synthetic PIV recording pair that has the same particle images as in the example in Sect. 2.3. but smaller amplitude of the particle image displacement, i.e.,

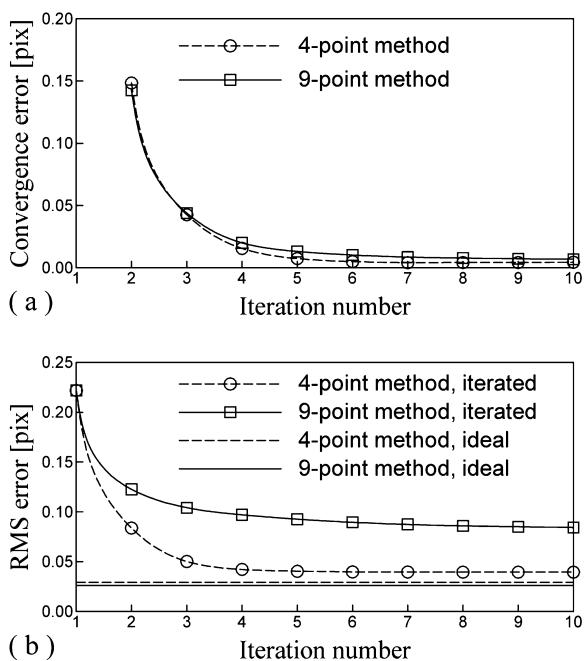


Fig. 3a, b. Convergence of the image correction methods

3 pixels. This synthetic recording pair is evaluated by combining the CDIC with the two correlation algorithms in a total of ten iterations (the RMS evaluation errors at different iterations are provided in Fig. 4). A 24×24 -pixel interrogation window is chosen for the correlation-based interrogation and a padding method is used to enable the FFT acceleration (Gui and Merzkirch 1998). For the correlation-based tracking, the first and second window are 24×24 and 32×32 pixels, respectively. Test results show that both algorithms converge in five iterations and an obviously lower evaluation error is achieved with the correlation-based interrogation.

A further test is conducted with synthetic PIV recordings of simulated four-roll mill flows (see Sect. 3) with different particle diameters. These synthetic recordings have a digital size of $1,024 \times 1,024$ pixels, a zero displacement in the center, and a maximal displacement magnitude of 10 pixels at the four corners. In each synthetic PIV recording pair, the particle images have the same diameter and brightness, but are distributed randomly. The average particle image density is $0.0098 \text{ pixel}^{-1}$, i.e., 10 in a 32×32 -pixel window. The evaluation of these synthetic recording pairs is conducted with a 32×32 -pixel interrogation window in two steps: In the first step, there are three iterations with a search radius of 12 pixels, i.e., the side length of the second sample window for the correlation-based tracking algorithms is $32 + (2 \times 12) = 56$ pixels; In the second step, there are two iterations with a search radius of 4 pixels. After analyzing the evaluation results, the dependence of the RMS evaluation errors on the particle image diameter is shown in Fig. 5 for CDIC with the correlation-based interrogation, CDIC with the correlation-based tracking, and the correlation-based tracking without CDIC. The RMS errors of the traditional correlation-based interrogation algorithm were computed in the first iteration cycle of the CDIC scheme, but they are too large to be plotted on the scale of Fig. 5, i.e., greater than 0.20 pixel. Test results in Fig. 5 show that in the traditional single-pass scheme, the evaluation error of the correlation-based interrogation (> 0.2 pixel) is much larger than that of the correlation-based tracking algorithm ($0.09 \sim 0.12$ pixel) in all the test cases. When combined with CDIC, both the bias and random error resulting from the image distortion are minimized, so that the total evaluation error of the

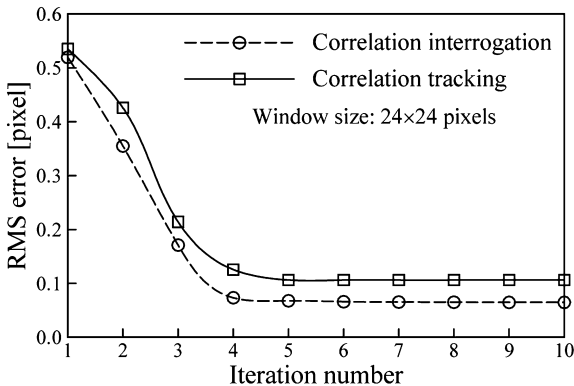


Fig. 4. RMS error distributions on the iteration number for two correlation schemes combined with CDIC

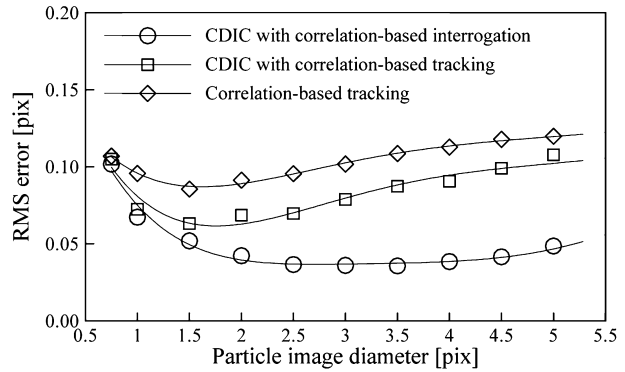


Fig. 5. Dependence of the RMS evaluation error on the particle image diameter

correlation-based tracking algorithm is further reduced. However, in the multi-pass, CDIC scheme, the correlation-based interrogation algorithm has a much lower error level than the correlation-based tracking algorithm. This can be explained with the automatically implemented continuous window shifting which enables a complete use of the high accuracy of the correlation-based interrogation algorithm near zero particle image displacement (Gui and Wereley 2002). In addition, Fig. 5 shows that the optimal particle image diameter is between 1 and 2 pixels in these test cases, agreeing with earlier results conducted by other researchers (e.g., Willert 1996). The limited optimal diameter range can be greatly extended to larger values (e.g., up to 5 pixels in this test) by basing the CDIC scheme on the correlation-based interrogation algorithm. This is of great importance in PIV measurements with high-resolution CCD cameras, or in micro-PIV tests, where the particle images are usually more than 3 pixels in diameter.

For further illuminating the advantage of the correlation-based interrogation over the correlation-based tracking algorithm in the CDIC evaluation scheme, a synthetic PIV recording pair is used to test the two algorithms with different interrogation window sizes. In this synthetic recording pair the average particle image number density is $0.0195 \text{ pixel}^{-1}$; the particle image diameter is 1 pixel, and the simulated flow is the same as for the previous test. The RMS errors of the two evaluation algorithms with interrogation windows varying from 8 to 64 pixels in side length are provided in Fig. 6. Test results in Fig. 6 show that the accuracy of the two algorithms is nearly the same for large interrogation windows, whereas the correlation-based interrogation algorithm has a lower evaluation error level for small interrogation windows. This implies that a higher spatial resolution can be achieved with correlation-based interrogation at the same accuracy level. Since the correlation-based tracking algorithm usually needs a much larger computation window when accelerated with FFT, it takes much more computation time than the correlation-based interrogation algorithm. A comparison of the computation time with a personal computer (Intel Celeron, 600 MHz) is given in Table 1. The value in Table 1 is the computation time for each evaluation vector during the five iterations. When using the FFT algorithm to accelerate the evaluation, the

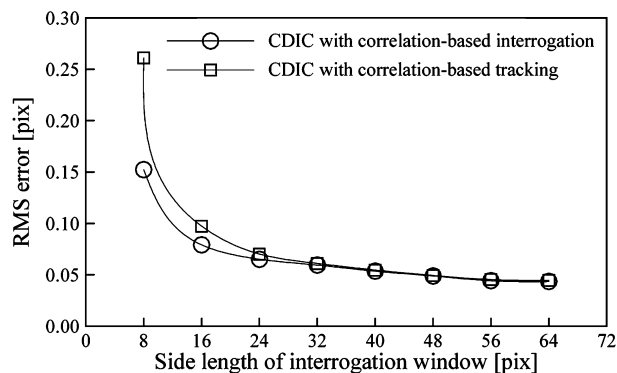


Fig. 6. Dependence of the RMS evaluation error on the interrogation window size

Table 1. Comparison of computation time

Interrogation window [pixels]	Computation time [ms/vector]	
	Correlation interrogation	Correlation tracking
8×8	8.062	38.29
32×32	11.84	57.19
64×64	28.97	279.2

Table 2. Computation windows

Interrogation window [pixels]	Computation window [pixels]	
	Iteration 1~3	Iteration 4~5
8×8	32×32/64×64	8×8/16×16
32×32	32×32/64×64	32×32/64×64
64×64	64×64/128×128	64×64/128×128

side length of the computation window for the correlation-based tracking should be power of two and not less than the interrogation window side length plus twice the search radius. The search radii used in the initial (1~3) and secondary (4~5) iteration cycles are 12 and 4 pixels, respectively, and the computation windows used in the time test are given in Table 2. Note that a 32×32-pixel interrogation window is used in the initial iteration cycles for the both algorithms in the case of 8×8-pixel interrogation window.

3 Application of CDIC in a four-roll-mill

3.1 Experiment setup

A top view of the four-roll mill device used for the test is shown in Fig. 7. It consists of four cylinder rollers of radius 7.2 mm, centered on the corners of a square of side length 12.04 mm immersed in a square tank. The height of the roller is 58 mm. The rotation of the cylinder rollers is controlled in steps with a gear system and the rotation angle for each step is 1.43×10^{-3} . The working fluid is polyisobutylene. Extendspheres (SF14) produced by PQ

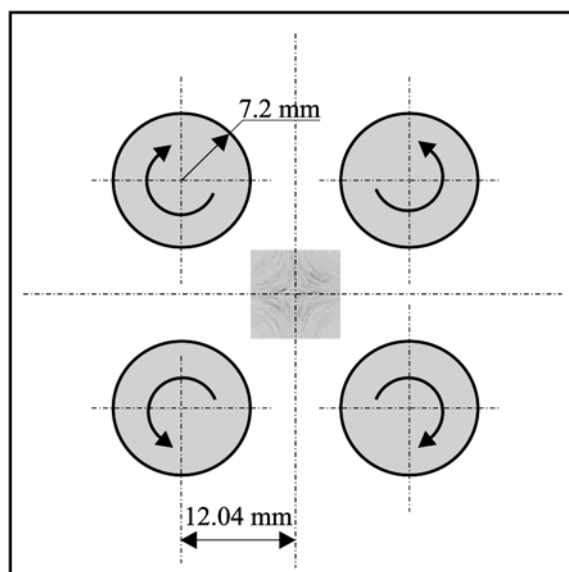


Fig. 7. Schematic diagram of the four-roll mill

Corporation (Philadelphia, Pa.) are used as tracer particles, which have a mean diameter of 55 μm and density of 0.74 g/cm^3 . The measurement area of 9.48×9.48 mm^2 centered among the four-roll mill is viewed by a Kodak ES1.0 camera with digital resolution of 1,008×1,008 pixels. The seeded flow is illuminated with a constant white light sheet. In the experiment, the rotation of the cylinders is controlled at rates between 10 and 800 steps per second (i.e., 0.1366~10.9244 rpm), so that desired flow patterns are generated. Particle images are recorded in successive frames with given time interval between 50~4,000 ms. The large time interval is suitable for the low roller speed and small time interval for the high speed, so that the maximal particle image displacement varies from 15 to 35 pixels.

Since the flow in the four-roll-mill is laminar and steady, the image pairs obtained in each test case are overlapped (Wereley et al. 2001) to avoid large errors resulting from the low particle image number density. As an example, the first image of the overlapped PIV recording pair for a cylinder rotation speed of 0.1366 rpm and $\Delta t=4$ s is shown in Fig. 8. Since in this case the velocity is very low and the PIV images are consecutively recorded, the streamlines of the four-roll mill flow are visualized clearly. The overlapped PIV recording pair in this case is evaluated using the CDIC method with a 64×64-pixel interrogation window and the results are given in Fig. 9 in form of velocity vectors. Figure 9 shows a symmetric flow pattern with low velocity in the center and high velocity at the corners, i.e., near to the rollers.

3.2 Evaluation errors of FDI and CDI

The four-roll mill is used to generate a two-dimensional pure extensional flow with velocity field $u=Ax$, $v=-Ay$. For a given fluid, A is a constant determined by the rotation speed of the rollers. In the first quadrant of the cartesian coordinate system, the streamlines in the four-roll mill can be described as

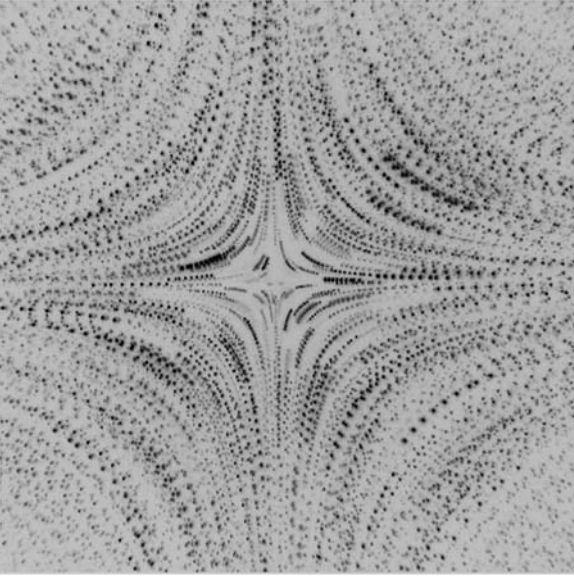


Fig. 8. Overlapped PIV images (inverted) from the four-roll mill flow

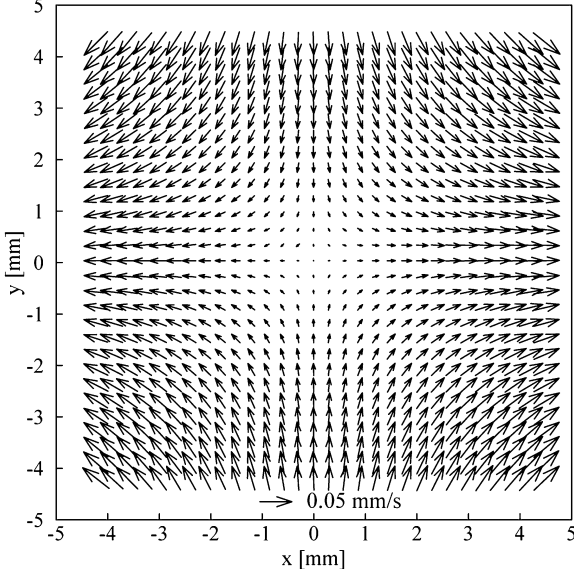


Fig. 9. Vector map of the four-roll mill flow at cylinder rotation speed of 10 steps/s

$$x(t) = Ge^{At}, \quad y(t) = Ge^{-At} \quad (3)$$

with the origin ($t=0$) at $(x=G, y=G)$, i.e., the intersection of the stream lines and line $x=y$. In the experiment, the velocity component u of a tracer particle located at position x can be approximately determined with the FDI and CDI, respectively, as

$$u_{\text{FDI}} = \frac{x(t + \Delta t) - x(t)}{\Delta t}, \quad (4)$$

$$u_{\text{CDI}} = \frac{x(t + \Delta t/2) - x(t - \Delta t/2)}{\Delta t}. \quad (5)$$

The bias errors of the two approximations is determined as follows:

$$\begin{aligned} \Delta u_{\text{FDI}} &= u_{\text{FDI}} - u = \frac{x(t)}{\Delta t} (e^{A\Delta t} - 1 - A\Delta t) \\ &= \frac{x(t)}{\Delta t} \left[\frac{1}{2} (A\Delta t)^2 + \frac{1}{4} (A\Delta t)^3 + \frac{1}{8} (A\Delta t)^4 + \dots \right], \quad (6) \\ &= Ax \sum_{n=1}^{\infty} \left(\frac{A\Delta t}{2} \right)^n = u \sum_{n=1}^{\infty} \left(\frac{A\Delta t}{2} \right)^n \end{aligned}$$

$$\begin{aligned} \Delta u_{\text{CDI}} &= u_{\text{CDI}} - u = \frac{x(t)}{\Delta t} \left(e^{A\Delta t/2} - e^{-A\Delta t/2} - A\Delta t \right) \\ &= \frac{x(t)}{\Delta t} \left[\frac{2}{4} \left(\frac{A\Delta t}{2} \right)^3 + \frac{2}{16} \left(\frac{A\Delta t}{2} \right)^5 + \frac{2}{64} \left(\frac{A\Delta t}{2} \right)^7 + \dots \right]. \quad (7) \\ &= Ax \sum_{n=1}^{\infty} \left(\frac{A\Delta t}{4} \right)^{2n} = u \sum_{n=1}^{\infty} \left(\frac{A\Delta t}{4} \right)^{2n} \end{aligned}$$

Similarly, the bias errors of the velocity component v are determined for FDI and CDI, respectively, as

$$\Delta v_{\text{FDI}} = -Ay \sum_{n=1}^{\infty} \left(\frac{-A\Delta t}{2} \right)^n = v \sum_{n=1}^{\infty} \left(\frac{-A\Delta t}{2} \right)^n, \quad (8)$$

$$\Delta v_{\text{CDI}} = -Ay \sum_{n=1}^{\infty} \left(\frac{-A\Delta t}{4} \right)^{2n} = v \sum_{n=1}^{\infty} \left(\frac{-A\Delta t}{4} \right)^{2n}. \quad (9)$$

Since $A\Delta t$ is usually a very small value, e.g., in the current test case $A\Delta t < 0.07$, and the bias error of CDI is in a higher order of the small value than that of FDI, the bias error of CDI is much smaller. Ignoring the higher order terms, the total bias errors approximated as follows:

$$\Delta V_{\text{FDI}} = \sqrt{(x^2 + y^2)(A^2\Delta t/2)^2} = \frac{A^2\Delta t}{2} r, \quad (10)$$

$$\Delta V_{\text{CDI}} = \sqrt{(x^2 + y^2)(A^3\Delta t^2/16)^2} = \frac{A^3\Delta t^2}{16} r. \quad (11)$$

Equations 10 and 11 indicate that the bias errors of the four-roll mill PIV tests are proportional to radius r . To confirm this assertion, 500 synthetic PIV recording pairs are generated according to the theoretical velocity distribution of the four-roll mill flow with 0.04 mm/s at the corner of the measurement area, where the corresponding particle image displacement is 30 pixels. The large number of image pairs are necessary to get good statistics. The particle images are similar to those in the real PIV recordings: diameter of 3~6 pixels, brightness of 100~250, particle image number of 10,240. These synthetic PIV recording pairs are, at first, evaluated with correlation-based FDI and CDI algorithms without image correction. The error distributions on the radial positions, obtained by statistically analyzing the evaluation results, are given in Fig. 10. The bias errors are determined by averaging individual error maps obtained through subtracting the known (given) displacement vectors from the evaluated vector maps. The random error is defined here as the root-mean-square (RMS) difference between the individual vectors and the mean at a certain evaluation spot. The total error is the root sum square (RSS) of the bias and the random error. As clearly shown in Fig. 10a, the bias error of FDI is a proportional function of the radial position. The bias error of CDI looks independent of the radial position (Fig. 10b) because its gradient is very small and

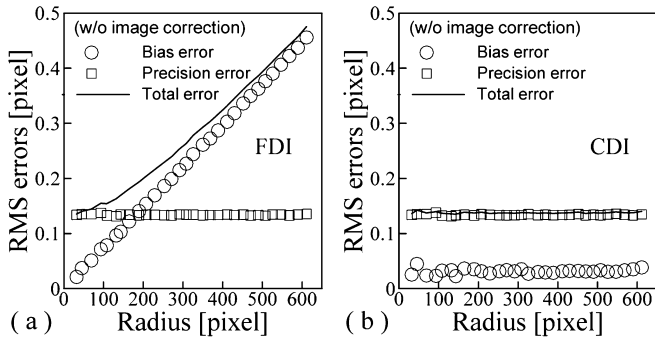


Fig. 10a, b. Dependencies of evaluation errors on the radial position for using *a* FDI and *b* CDI without image correction

within the bias error variation that results from the limited sample number for the statistical analysis. Figure 10 also shows that the random (precision) errors of FDI and CDI are on the same level and independent of the radial position. For FDI, the total error is dominated by the bias error at radial positions greater than 200 pixels, whereas for CDI, the random error dominates in the whole area.

3.3 Effect of the image correction

The random error level shown in Fig. 10 is very high and cannot be reduced by replacing FDI with CDI. However, using the image correction technique can effectively reduce the random evaluation error. In order to demonstrate the effects of the image correction method on the evaluation errors, the 500 synthetic PIV image pairs are again evaluated with the FDI and CDI algorithm, but in combination with the four-point image correction method. The results in Fig. 11 indicate that the image correction does not noticeably change the bias error distribution, but effectively reduces the random (precision) evaluation error (here, by half).

3.4 Reduction of peak-locking effect with CDIC

The peak-locking effect continues to be a big problem when evaluating digital PIV recordings, especially in the investigations of turbulent structure and vorticity distribution. Gui and Wereley (2002) discussed the mechanism of the peak-locking phenomenon in detail and suggested a

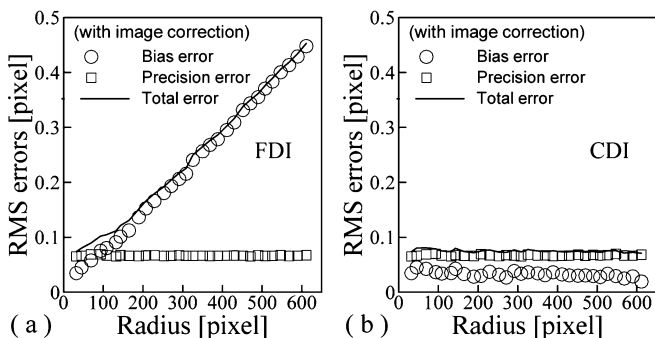


Fig. 11a, b. Dependencies of evaluation errors on the radial position for using *a* FDI and *b* CDI with image correction

continuous window-shifting technique to minimize the peak-locking effect. They found that the worst peak-locking case is to combine the correlation-based interrogation algorithm with discrete window shifting. However, the CDIC technique avoids this discrete window shifting. It is equivalent to the continuous window-shifting technique when there is no image distortion. As an example, the histograms of the evaluated particle image displacements using the discrete central difference interrogation (DCDI) and the CDIC method are given in Fig. 12 for the overlapped PIV recording pair in the case of cylinder rotation speed of 0.1366 rpm and $\Delta t=4$ s. Theoretically, the histograms should be flat and smooth, because the distribution of the velocity components in the four-roll mill is uniform. However, as shown in Fig. 12a, the particle image displacements obtained with the DCDI method are obviously concentrated toward integer pixels, so that a very strong peak-locking effect is observed. Figure 12a also shows that the peaks at even pixel numbers are higher than these at odd pixel numbers. This phenomenon results from the DCDI scheme, with which the bias and random error distribution on the particle image displacement has a 2-pixel period. When using the CDIC method, the strong peak-locking effect cannot be observed anymore (Fig. 12b).

3.5 Experiment results

The direct (raw) results of the four-roll mill PIV tests are velocity vector maps. With a quantitative analysis of the vector maps the distributions of the velocity components (u , v) on the coordinates (x , y) can be experimentally determined for different test cases. Since the evaluation of the PIV recording pairs are conducted on a 30×30 uniform grid structure, in each column and each row, 30 values are used to determine the mean and standard deviation of u and v , respectively. Figure 13 provides the post-processed results for the test case of a cylinder rotation speed of

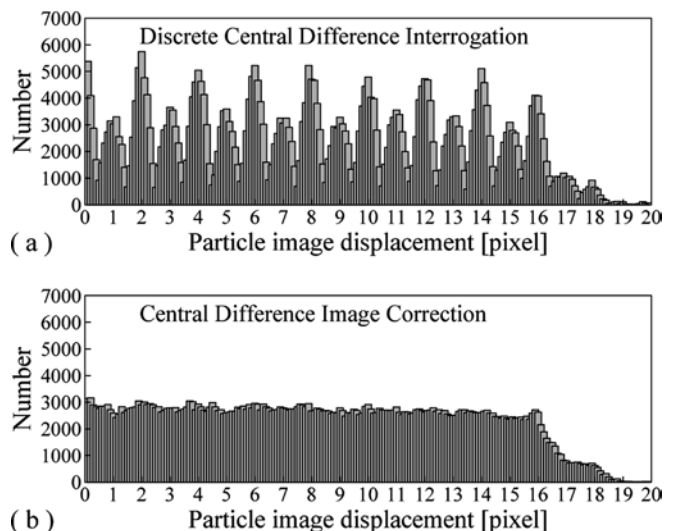


Fig. 12a, b. Histograms of the particle image displacements in a four-roll mill test case using *a* the discrete CDI and *b* the CDIC method

5.4622 rpm. In the figure, the error bars show the precision error, i.e., twice the standard deviation for a 95% confidence level, and the two lines are least square fits of the mean values of u and v , respectively. In this case, the experimentally determined factor A has a difference of 0.0007 [1/s] (i.e., 0.2% in relative terms) between the two coordinate directions, which can be explained as the misalignment of the PIV camera view. The experimentally determined factor A and its bias error bar are given in Fig. 14 for three test cases with different cylinder rotation speeds. It is shown that the factor A is a linear function of the cylinder rotation speed. The error bars represent the bias errors resulting from the misalignment of the PIV camera view.

4 Summary and conclusions

The CDIC method described in this paper combines features of the CDI, image pattern correction, and continuous window shifting. Using this algorithm for evaluating digital PIV recordings can minimize bias errors resulting from curvature and high-velocity-gradient flows, effectively reduce the random evaluation error caused by the image pattern distortion, and avoid strong peak-locking effects. As a multi-pass algorithm, four to five iterations are usually necessary for using the CDIC method to get an accurate, converged result. In comparison to the adaptive discrete window-shifting techniques with the same com-

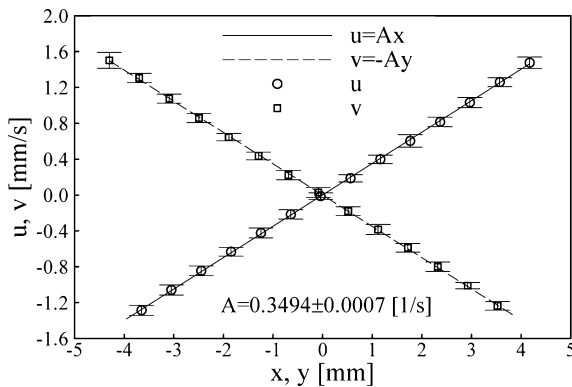


Fig. 13. Distributions of mean velocity components and precision errors in the four-roll mill at cylinder speed of 400 steps/s

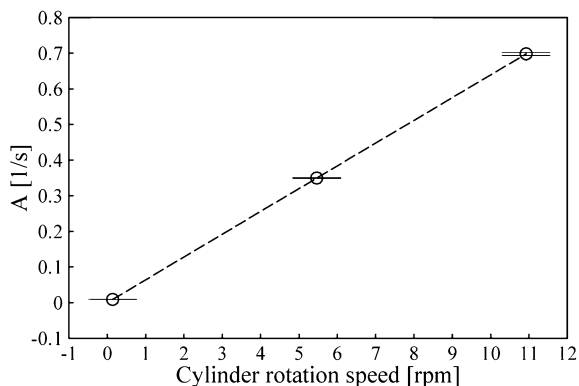


Fig. 14. Dependence of factor A on the cylinder rotation speed

putation window, the CDIC method needs about 75% more computation time. When using the CDIC method, the continuous window shifting is automatically implemented, so that the strong peak-locking effects of the correlation-based adaptive discrete window-shifting technique is avoided.

In the present work, a bilinear image interpolation scheme is used in CDIC to enable a stable and fast computation. Because of its simplicity, considerable error may be added to the evaluation when the particle images are too small. However, a test indicates that the error added by this interpolation scheme is less than 10% of evaluation error of the conventional correlation-based interrogation algorithm when the diameter of the particle images is not smaller than 2 pixels.

A four-point image correction scheme is suggested for the CDIC method in combination with the correlation-based interrogation algorithm. Theoretically, a higher accuracy might be achieved when using the particle image displacements of nine or more points in the interrogation window to correct the distorted image pattern. However, the evaluation error of the four-point scheme converges to a much lower level error than that of the nine-point scheme. This may be explained by that the additional degrees of freedom in the nine-point fit allow the particle image patterns to be matched well in the presence of small displacement deviations. Further study of the image correlation schemes seems to be necessary to optimize the CDIC method. Investigations show that when combining CDIC with the correlation-based interrogation algorithm, both higher evaluation accuracy and much lower computational cost can be achieved than when combining CDIC with the correlation-based tracking algorithm.

The PIV experiment accurately determines the velocity field in the four-roll mill and confirms the linear distributions of the velocity components on the coordinates and the roller speed. The test results are valuable for understanding the four-roll mill flow and developing new devices.

References

- Bentley BJ, Leal LG (1986a) An experimental investigation of drop deformation and breakup in steady, two-dimensional linear flows. *J Fluid Mech* 167:241
- Bentley BJ, Leal LG (1986b) A computer-controlled four-roll mill for investigation of particle and rope dynamics in two-dimensional linear shear flows. *J Fluid Mech* 167:219
- Cowen EA, Monismith SG (1997) A hybrid digital particle-tracking velocimetry technique. *Exp Fluids* 22:199–211
- Fincham AM, Spedding GR (1997) Low-cost, high-resolution DPIV for measurement of turbulent fluid flow. *Exp Fluids* 23:449–462
- Gui L, Merzkirch W (1996) Phase-separation of PIV digital mask technique. *ERCOFTAC Bull* 30:45–48
- Gui L, Merzkirch W (1998) Generating arbitrarily sized interrogation windows for correlation-based analysis of particle image velocimetry recordings. *Exp Fluids* 24:66–69
- Gui L, Merzkirch W (2000) A comparative study of the MQD method and several correlation-based PIV evaluation algorithms. *Exp Fluids* 28:36–44
- Gui L, Wereley ST (2002) A correlation-based continuous window shift technique for reducing the peak-locking effect in digital PIV image evaluation. *Exp Fluids* 32:506–517
- Guller GG, Leal LG (1981) Flow birefringence of concentrated polymer solutions in two-dimensional linear flows. *J Polym Sci Polym Phys* 19:557

- Higdon JLL (1993) The kinematics of the four-roll mill. *Phys Fluids A* 5:274–276
- Huang HT, Fiedler HE, Wang JJ (1993) Limitation and improvement of PIV. Part II: particle image distortion, a novel technique. *Exp Fluids* 15:263–273
- Keane RD, Adrian RJ (1993) Theory and simulation of particle image velocimetry. *Proc SPIE (Laser anemometry advances applications)* 2052:477–492
- Lecordier B, Demare D, Vervisch LMJ, Reveillon J, Trinite M (2001) Estimation of the accuracy of PIV treatments for turbulent flow studies by direct numerical simulation of multi-phase flow. *Meas Sci Tech* 12:1382–1391
- Lin HJ, Perlin M (1998) Improved methods for thin, surface boundary layer investigations. *Exp Fluids* 25:431–444
- Nogueira J, Lecuona A, Rodriguez PA (1999) Local field correction PIV: on the increase of accuracy of digital PIV systems. *Exp Fluids* 27:107–116
- Nogueira J, Lecuona A, Rodriguez PA (2001) Local field correction PIV, implemented by means of simple algorithms, and multigrid versions. *Meas Sci Tech* 12:1911–1921
- Rumscheidt FD, Masno SG (1961) Particle motions in sheared suspensions XI. Internal circulation in fluid droplets (Experimental). *J Colloid Sci* 16:210
- Scarano F (2002) Iterative image deformation methods in PIV. *Meas Sci Tech* 13:R1–R19
- Scarano F, Riethmuller ML (1999) Iterative multigrid approach in PIV image processing with discrete window offset. *Exp Fluids* 26:513–523
- Scarano F, Riethmuller ML (2000) Advances in iterative multi-grid PIV image processing. *Exp Fluids* 29:51–60
- Sholl MJ, Savas Ö (1997) A fast Lagrangian PIV method for study of general high gradient flow. AIAA paper 97–0493 (A97–15543). Reston, Va.
- Sjödahl M (1994) Electronic speckle photography: increased accuracy by nonintegral pixel shift. *Appl Opt* 33:6667–6673
- Taylor GI (1934) The formation of emulsions in definable fields of flow. *Proc R Soc Lond Ser A* 146:501
- Tokumaru PT, Dimotakis PT (1995) Image correlation velocimetry. *Exp Fluids* 19:1–15
- Torza S (1975) Shear-induced crystallization of polymers; I: the four-roller apparatus. *J Polym Sci Polym Phys* 13:43
- Wereley ST, Meinhart CD (2000) Accuracy improvements in particle image velocimetry. In: 10th International Symposium on Applications of Laser Techniques to Fluid Mechanics, July 2000, Lisbon, Portugal, paper 13.4
- Wereley ST, Meinhart CD (2001) Second-order accurate particle image velocimetry. *Exp Fluids* 31:258–268
- Wereley ST, Santiago JG, Meinhart CD, Adrian RJ (1998) Velocimetry for MEMS Applications. In: Forster FK, Breuer K, Bandyopadhyay P (eds) *Proc. of ASME/DSC, Vol. 66, Micro-fluidics symposium*, November 1998, Anaheim, Calif., pp 453–459
- Wereley ST, Gui L, Meinhart CD (2001) Flow measurement techniques for the microfrontier. In: 30th Aerospace Science Meeting & Exhibit, 8–11 January 2001, Reno, Nev., paper AIAA 2001-0243
- Westerweel J, Dabiri D, Gharib M (1997) The effect of a discrete window offset on the accuracy of cross-correlation analysis of digital PIV recordings. *Exp Fluids* 23:20–28
- Willert CE (1996) The fully digital evaluation of photographic PIV recordings. *Appl Sci Res* 56:79–102